The Cryosphere Discuss., https://doi.org/10.5194/tc-2018-205
Manuscript under review for journal The Cryosphere
Discussion started: 11 October 2018

The Cryosphere Discussions
Open Access
EGU

A simple stress-based cliff-calving law

Tanja Schlemm[1,2] and Anders Levermann[1,2,3]

[1]Potsdam Institute for Climate Impact Research, Potsdam, Germany
[2]Institute of Physics and Astronomy, University of Potsdam, Potsdam, Germany
[3]Lamont-Doherty Earth Observatory, Columbia University, New York, USA

Correspondence: Anders Levermann (anders.levermann@pik-potsdam.de)

Abstract. Over large coastal regions in Greenland and Antarctica the ice sheet calves directly into the ocean. In contrast to ice-shelf calving, an increase in cliff calving directly contributes to sea-level rise and a monotonously increasing calving rate with ice thickeness can constitute a self-amplifying ice loss mechanism that may significantly alter sea-level projections both of Greenland and Antarctica. Here we seek to derive a minimalistic stress-based parameterization for cliff calving. To this end we compute the stress field for a glacier with a simplified two-dimensional geometry from the two-dimensional Stokes equation. First we assume a constant yield stress to derive the failure region at the glacier front from the stress field within the ice sheet. Secondly, we assume a constant response time of ice failure due to exceedance of the yield stress. With this strongly constraining but very simple set of assumption we propose a cliff-calving law where the calving rate follows a power-law dependence on the freeboard of the ice with exponents between 2 and 3 depending on the relative water depth at the calving front. The critical freeboard below which the ice front is stable decreases with increasing relative water depth of the calving front. For a dry water front it is, for example, 75m. The purpose of this study is not to provide a comprehensive calving law, but to derive a particularly simple equation with a transparent and minimalistic set of assumptions.

1 Introduction

Ice loss from Greenland and Antarctica is increasingly contributing to global sea-level rise (Rignot et al., 2014; Shepherd et al., 2018; WCRP Global Sea Level Budget Group, 2018). A possible future mass loss from these ice sheets is of crucial importance for future sea-level projections (Slangen et al., 2017; Church et al., 2013; DeConto and Pollard, 2016; Kopp et al.; Mengel et al., 2016; Ritz et al., 2015; Levermann et al., 2014). Calving accounts for roughly half the ice loss of the Antarctic ice shelves, the rest is lost by basal melt (Depoorter et al., 2013). For the Greenland ice sheet, calving accounted for two-thirds of the ice loss between 2000 and 2005, the rest is due to enhanced surface melting and runoff (Rignot and Kanagaratnam, 2006). Because surface melt increased faster than glacier speed, calving accounted for one-third of the Greenland ice sheet between 2009 and 2012 (Enderlin et al., 2014).

The Cryosphere Discuss., https://doi.org/10.5194/tc-2018-205
Manuscript under review for journal The Cryosphere
Discussion started: 11 October 2018

Tidewater glaciers calve vigorously when they are near floatation thickness producing icebergs with a horizontal extend smaller than the ice thickness. This has been expressed in semi-empirical height-above-floatation calving laws (Meier and Post, 1987; van Der Veen, 1996; Vieli et al., 2002). Calving at ice-shelf fronts or floating glacier tongues has long rest periods interupted by the calving of large tabulare ice bergs (Lazzara et al., 1999) and is preceded by the formation of deep crevasses upstream (Joughin and MacAyeal, 2005). The distinction between these two kinds of calving is not always easy because a tidal glacier can form or lose a floating tongue; this has for example been observed at the Columbia glacier in Canada (Walter et al., 2010).

In order to model calving not just for single glaciers but for whole ice sheets, a calving parametrization is needed. Theories describing the nucleation and spreading of crevasses in ice (Pralong and Funk, 2005) are computationally very intense and difficult to apply in simulations on long timescales and large spatial dimensions. In order to parameterize calving processes several approaches have been used:

First, calving can be described as a function of strain rate and crevasse depth. Nye (1957) first described the formation of crevasses as a result of velocity gradients: The depth of the crevasse is determined by the strain-rate and overburdening pressure of the ice. Observations show that ice velocities are greater near the calving front than upstream (Meier and Post, 1987), hence crevasses form mainly at the calving front. When crevasses are deep enough, icebergs are separated from the glacier and calve off. Benn et al. (2007) proposed a calving law with the assumption that a glacier calves where crevasses reach the water level, Nick et al. (2010) proposed calving when surface and basal crevasses meet. These calving laws have been applied successfully in 1D flowline models Nick et al. (2010) and in a 3D Full Stokes model (Todd et al., 2018).

Second, a number of approaches have been taken to analyze calving processes via the stress balance. Bassis and Walker (2011) analyzed depth-averaged stresses at the calving front. Considering tensile and shear failure, they found that there is an upper thickness limit for stable ice cliffs: an ice cliff is only stable if the glacier freeboard (ice thickness minus water depth) is lower than 200m. The limit decreases to 100m if weakening of the ice through crevasses is also considered. More recent works by Ma et al. (2017) and Benn et al. (2017) solved the 2D full-Stokes equation at the calving front with finite element methods. Ma et al. (2017) found that while sliding glaciers calve through tensile failure, for glaciers frozen to the bed shear failure dominates. Benn et al. (2017) used finite element models to solve the stress balance and a discrete element model to model fracture formation. They modelled a range of calving mechanisms including calving driven by buoyancy and melt-undercutting.

Finally, Mercenier et al. (2018) analysed tensile failure with 2D finite elements and derived a calving law for tidewater glaciers. All these approaches aggree on the basic physics of glacier calving: Thicker ice at the terminus leads to higher stresses and larger calving rates. Glaciers terminating in water are stabilized by the water's back-pressure and have smaller calving rates.

The stability limit derived by Bassis and Walker (2011) lead to the formation of the marine ice cliff instability hypothesis. Here, cliff calving means calving from ice cliffs whose freeboards exceed the stability limit. If cliff calving is initiated in an overdeepend basin, e.g. in East Antarctica, it can lead to runaway cliff calving where higher ice cliffs are exposed the further the grounding line retreats, causing even larger cliff calving rates.

The Cryosphere Discuss., https://doi.org/10.5194/tc-2018-205
Manuscript under review for journal The Cryosphere
Discussion started: 11 October 2018

Pollard et al. (2015) and DeConto and Pollard (2016) incorporated cliff calving in Antarctica projections by assuming a linear relation between freeboard exceeding the stability limit and calving rate and showed that the marine ice cliff instability can lead to faster sea level rise than expected. More research is needed and especially a more physically based cliff calving law. Studies by Ma et al. (2017), Benn et al. (2017) and Mercenier et al. (2018) were made for tidewater glaciers not exceeding the stability limit and it is not clear what a cliff calving law would look like.

In this study, we analyse stresses at the calving front by solving the 2D Stokes equation with a finite element model in order to propose a simple cliff calving law. The purpose of this study is not to provide a comprehensive analysis. By contrast, we see a minimalistic set of assumptions that paths the way to a stress-based calving law.

2 Stress balance near the calving front

2.1 Problem set-up: 2D Stokes equation and boundary condition

In this study we consider a plane, flat glacier of constant thickness H terminating in water of depth D in a one-dimensional (flowline) model with horizontal coordinate x and vertical coordinate z (Figure 1). In order to compute the stress field near the calving front we set the glacier to be grounded (relative water depth $w \equiv D/H < 0.9$) and frozen to the bed. The numerical domain has a length of $L = 6 \cdot H \gg H$. The factor 6 was chosen as a compromise to reduce computational effort while ensuring that the upstream boundary does not effect stresses at the glacier terminus. L could have been chosen to be truly "much larger" than H but that would have required a lot of computation time without significantly benefiting the precision of the calculation. The flowline assumption is justified, for example, in situations where the glacier is wide in comparison to its length and thickness. In these cases lateral stresses can often be neglected. The flow line assumption is a strong constraint which neglects, for example, any buttressing effects within the ice sheet. However, the considered geometry with the width been much larger than the horizontal extent in flow direction L and the flow-line direction been $L = 6 \cdot H$ is internally consistent and applicable to a number of situations observed both in Greenland and Antarctica. The assumption of a flat ice thickness is justifiable on a horizontal scale of several hundred meters to a few kilometers.

The ice flow and the stresses within the ice are governed by the Stokes

$$\partial_x \sigma_{xx} + \partial_z \sigma_{xz} = 0 \tag{1}$$

$$\partial_x \sigma_{zx} + \partial_z \sigma_{zz} = f \tag{2}$$

and the continuity equations

$$\nabla \cdot \boldsymbol{u} = \partial_x u_x + \partial_z u_z = 0 \tag{3}$$

with the Cauchy stress tensor σ and the gravitational force f. The Cauchy stress tensor can be split into an isotropic pressure P (also called cryostatic pressure) and the deviatoric stress tensor S, such that

$$\sigma_{ij} = -P \cdot \delta_{ij} + S_{ij} \tag{4}$$

The Cryosphere Discuss., https://doi.org/10.5194/tc-2018-205
Manuscript under review for journal The Cryosphere
Discussion started: 11 October 2018

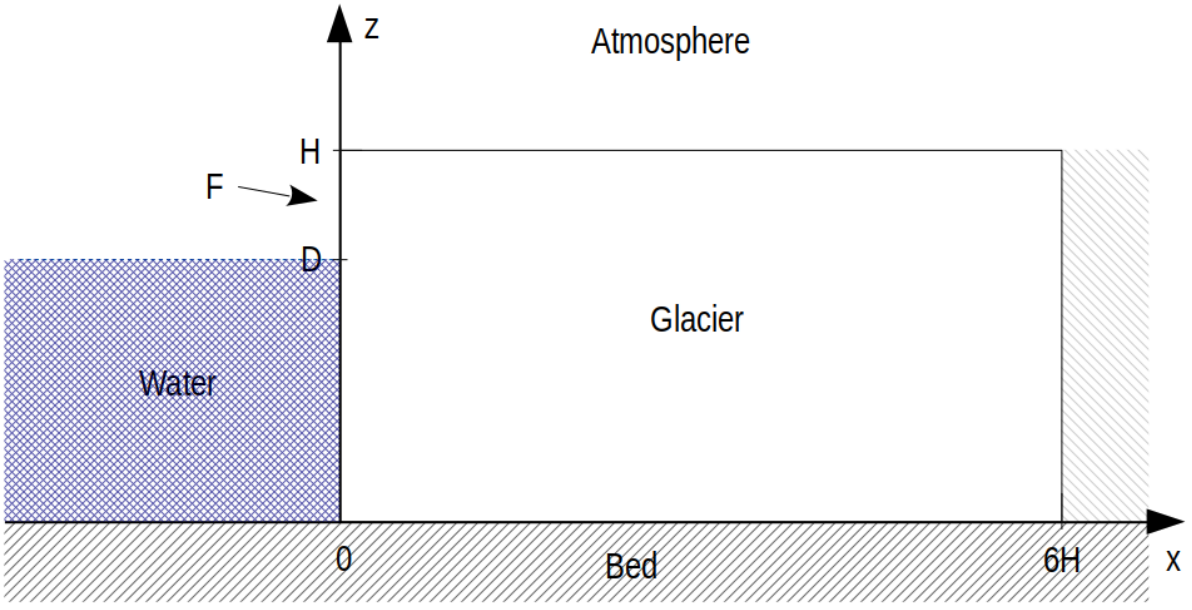

Figure 1. Geometrical set-up of the stress computation: two-dimensional plane flat glacier frozen to the bedrock with a calving front at its terminus. The glacier length L is six times as large as the glacier height H in order to ensure that the boundary condition on the right does not significantly influence the stress field at the terminus on the left. The ice thickness is denoted H, ice thickness below the water level is D and the free-board is denoted F.

where δ_{ij} is the Kronecker delta. Ice rheology is assumed to be given by Glen's flow law (van der Veen, 1999),

$$\dot{\epsilon}_{ij} = A S_e^{n-1} S_{ij}\,, \tag{5}$$

with the strain rate tensor $\dot{\epsilon}_{ij} = \frac{1}{2}\left(\partial_i u_j + \partial_j u_i\right)$ and the effective stress $S_e = \sqrt{\frac{1}{2}S_{xx}^2 + \frac{1}{2}S_{zz}^2 + S_{xz}^2}$.

The surface boundary is assumed to be traction-free. At the calving front boundary, we assume traction continuity to the water pressure and no traction above the water line. At the glacier bed, a no-slip boundary condition is assumed, which corresponds to a glacier frozen to its bed.

ice top: $$\sigma \cdot \boldsymbol{n} = \begin{pmatrix} \sigma_{xz} \\ \sigma_{zz} \end{pmatrix} = \mathbf{0}, \tag{6}$$

ice base: $$\boldsymbol{u} = \mathbf{0}, \tag{7}$$

ice front: $$\sigma \cdot \boldsymbol{n} = \begin{pmatrix} -\sigma_{xx} \\ -\sigma_{xz} \end{pmatrix} = \begin{cases} (-\rho_w g z, 0), & z < D \\ (0,0), & z > D \end{cases} \tag{8}$$

The Cryosphere Discuss., https://doi.org/10.5194/tc-2018-205
Manuscript under review for journal The Cryosphere
Discussion started: 11 October 2018

2.2 Numerical solution of the stress field

The boundary value problem was solved with the Finite Element package FEniCS (Alnæs et al., 2015) and stabilized with the Pressure Penalty method (Zhang et al., 2011). The numerical domain was divided into a regular triangular mesh with 100 vertical and 600 horizontal divisions. Since the Stokes equation is linear in the stresses and the terminus boundary condition is linear in the ice thickness, the equations can be solved on a dimensionless domain and the stresses scaled to arbitrary ice thickness. Velocities do not scale linearly but can be obtained from the scaled stresses through the ice rheology equation. The water depth at the calving front was incorporated via the relative (dimensionless) water depth $w = D/H$.

In order to determine a suitable stress-criterion for cliff calving we consider a number of commonly used stresses which have a clear physical role (figure 2). In general, we find that stresses increase with ice thickness, while the presence of water at the glacier terminus decreases the stresses and stabilizes the calving front. The deviatoric normal stress, S_{xx}, corresponds to an outwards force at the calving front which has two maxima, one at the waterline and one at the foot of the terminus. The deviatoric shear stress or Cauchy shear stress, ($S_{xz} = \sigma_{xz}$), translates to a bending moment which bends the top of the calving front forward and downward. The largest principal stress,

$$\sigma_1 = \frac{\sigma_{xx} + \sigma_{zz}}{2} + \sqrt{\left(\frac{\sigma_{xx} - \sigma_{zz}}{2}\right)^2 + \sigma_{xz}^2}\,, \tag{9}$$

is calculated as the largest eigenvalue of the Cauchy stress tensor and corresponds to the largest normal stress in a given point. When σ_1 is positive, it is tensile and crevasses can form. The maximum shear stress,

$$\tau_{max} = \sqrt{\left(\frac{\sigma_{xx} - \sigma_{zz}}{2}\right)^2 + \sigma_{xz}^2}\,, \tag{10}$$

acts on a plane at an angle $45°$ to the plane where the largest principal stress acts. It has its maximum at the foot of the calving front. The maximum shear stress can be related to brittle compressive failure (Schulson, 2001) and is therefore of particular interest for cliff failure. The von Mises stress,

$$\sigma_{Mises} = \sqrt{\frac{3}{2}\left(S_{xx}^2 + S_{yy}^2 + 2S_{xy}^2\right)}\,, \tag{11}$$

is a measure of deviatoric strain energy. It can also be related to material failure and has been used as a calving criterion by Morlighem et al. (2016). Its distribution (not shown) is very similar to that of the maximum shear stress.

3 Cliff failure criterion

In a first step we select a failure criterion which then yields a failure region based on the computed stress fields. In a second step we decide on a time scale for the failure in order to derive a simple calving law.

3.1 Partial thickness failure through crevasses

Crevasses are a natural candidate for ice front failure. In the case of glaciers that are frozen to the ground, crevasses, generally, do not form from the base upward (Ma et al., 2017). Instead, surface crevasses can form in the upper part of the glacier down

The Cryosphere Discuss., https://doi.org/10.5194/tc-2018-205
Manuscript under review for journal The Cryosphere
Discussion started: 11 October 2018

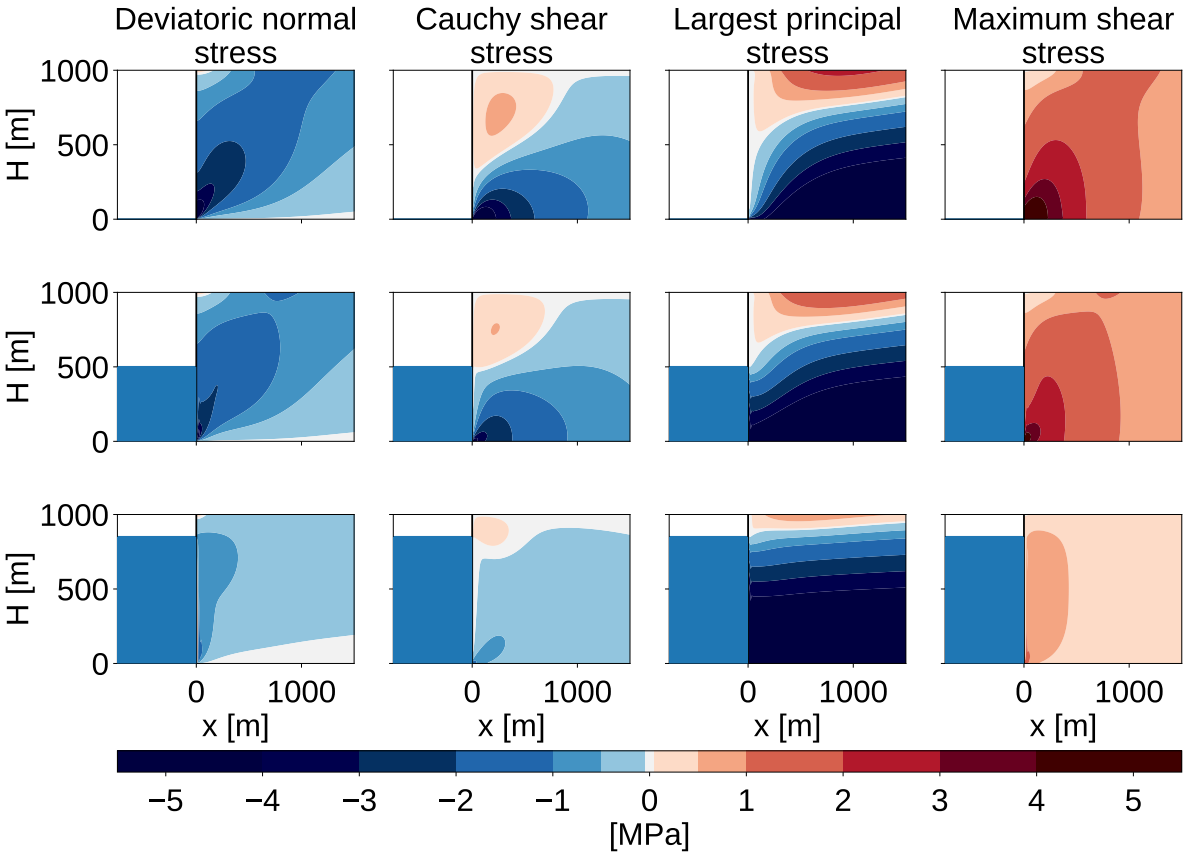

Figure 2. Stress configurations at the calving front for different relative water depths ($w = 0, 0.5, 0.85$) for a fixed ice thickness of 1000m. The first column shows the deviatoric normal stress in x-direction, S_{xx}, the second column shows the Cauchy shear stress, $\sigma_{xz} = S_{xz}$, the third column shows the largest principal stress, σ_i, and the last column shows the maximum shear stress, τ_{max}.

to the depth where the principal stress becomes compressive, i.e. attains negative values (Nye, 1957). The presence of water at the calving front reduces the stresses in the ice and decreases the depth to which surface crevasses can penetrate. Surface crevasses, generally, do not penetrate through the whole glacier thickness and so crevasses cannot be the sole cause for calving. We thus do not follow this path to determine a failure region. Surface meltwater filling surface crevasses can increase their depth (hydrofracturing) (Weertman, 1973; Das et al., 2008; Pollard et al., 2015), but this is also not considered here. The presence of crevasses weakens the ice and is expected to enable failure even when the critical shear stress is not yet exceeded but also this is not further considered here. Instead we consider the case of

3.2 Full thickness shear failure

The different components of the deviatoric stress tensor are no invariants of the stress tensor, i.e. they depend on the coordinate system in which they are computed, and therefore they are not suitable as failure criteria. The von-Mises stress is the second

The Cryosphere Discuss., https://doi.org/10.5194/tc-2018-205
Manuscript under review for journal The Cryosphere
Discussion started: 11 October 2018

invariant J_2 of the deviatoric stress tensor and is frequently used as a failure criterion in material sciences (Ford and Alexander, 1963). However, it does not take into account whether deviatoric stresses are tensile or compressive or shear stresses and this is likely to be important for ice failure.

Here, we assume shear faulting to be the dominant process in ice-cliff failure. The failure region is defined as the region close to the calving front where the maximum shear stress exceeds a critical shear stress of $\tau_c = 1\,\mathrm{MPa}$ (Schulson et al., 1999; Schulson, 2001). While the specific value of the critical shear stress may be subject to large uncertainties, it is mainly a constant that will not alter the calving rate dependence on the freeboard and the water depth. The specific choice of the value is motivated by laboratory experiments and can only provide an order of magnitude of the calving rate. However, the uncertainty resulting from this choice is probably not larger than the uncertainty arising from the estimate of the failure time (see below).

3.3 Comparison to Coulomb failure

In general, brittle compressive failure happens through shear faulting (Schulson et al. (1999)) and can be described with the Coulomb law (Weiss and Schulson (2009)): the shear stress τ acting on the future fault plane is resisted by material cohesion S_0 and by friction $\mu\sigma$ with the friction coefficient μ and the normal stress across the failure plane σ. Failure happens, when:

$$\tau \geq S_0 + \mu\sigma \tag{12}$$

This can be expressed in terms of the maximum shear stress τ_{max} and the isotropic pressure P as

$$\sqrt{\mu^2 + 1}\,\tau_{max} = \tau_0 + \mu P \tag{13}$$

where τ_0 is another measure of cohesive strength related to S_0.

Weiss and Schulson (2009) provide values of $\mu = 0.3 \ldots 0.8$ depending on the temperature of the ice. Since friction increases the strength of the ice, this could stabilize rather large ice cliffs. Bassis and Walker (2011) looked at upper bounds of glacier stability with a depth-averaged shear stress for different values of μ (0.65, 0.4, 0) and a cohesion of $\tau_0 = 1\,\mathrm{MPa}$. With a large friction coefficient, ice cliffs would be stable for freeboards of up to $600\,\mathrm{m}$ (see fig. 3) Since this is not observed in nature, they concluded that the best model is the one without friction which only allows freeboards of up to $200\,\mathrm{m}$. Thus with vanishing friction, the Coulomb failure criterion is equal to the maximum shear stress criterion used here.

4 Failure region

The maximum horizontal extend L of the failure region was determined for a range of ice thicknesses H and relative water depths w by solving the 2D Stokes equation numerically and tracing the contour line where the maximum shear stress τ_{max} equals the critical shear stress τ_c (see figure 4).

For a given water depth, the extent of the failure region increases with the ice thickness H or the glacier freeboard $F = H - D$ (figure 5). For glacier freeboards smaller than approximately 100m, the failure region vanishes: the critical shear stress is not exceeded anywhere in the ice and no shear failure takes place. This confirms results by Bassis and Walker (2011) which were

The Cryosphere Discuss., https://doi.org/10.5194/tc-2018-205
Manuscript under review for journal The Cryosphere
Discussion started: 11 October 2018

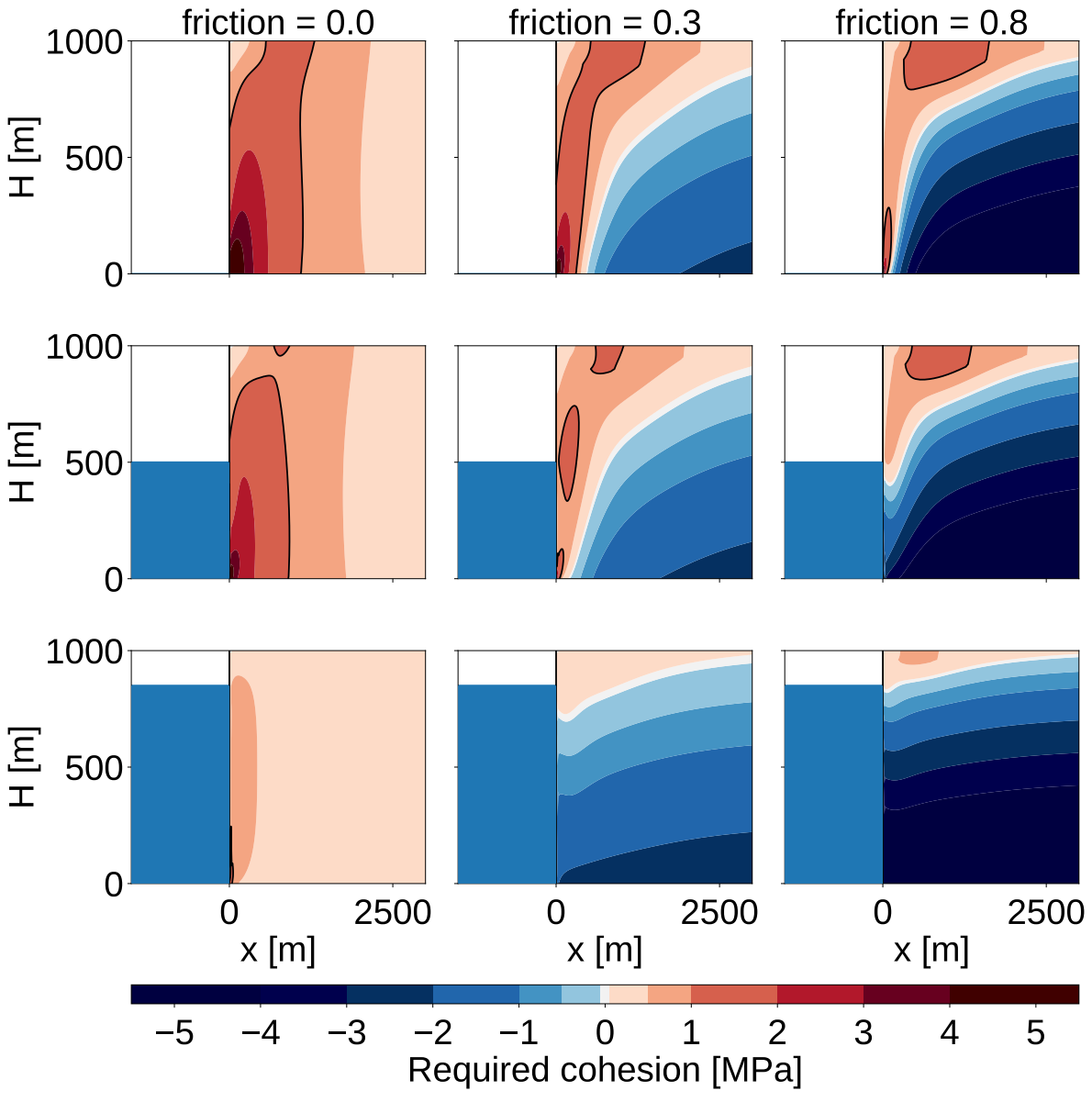

Figure 3. Assumin Coulomb failure, the required cohesion, $\tau_0 = \sqrt{\mu^2 + 1}\,\tau_{max} - \mu P$, is shown for different friction parameters ($\mu = 0, 0.3, 0.8$). The failure regionm for a maximum cohesion of $\tau_{max} = 1$ Mpa is encased by the black line.

derived analytically with some simplifications (see appendix A1 for more details). The relative water depths influences the slope of the freeboard - failure region relation: for large relative water depths, the failure region grows more quickly with increasing freeboard. This is because for a large relative water depth the overall ice thickness is much larger than for a similar freeboard with a smaller relative water depth and so the failure region is larger.

The Cryosphere Discuss., https://doi.org/10.5194/tc-2018-205
Manuscript under review for journal The Cryosphere
Discussion started: 11 October 2018

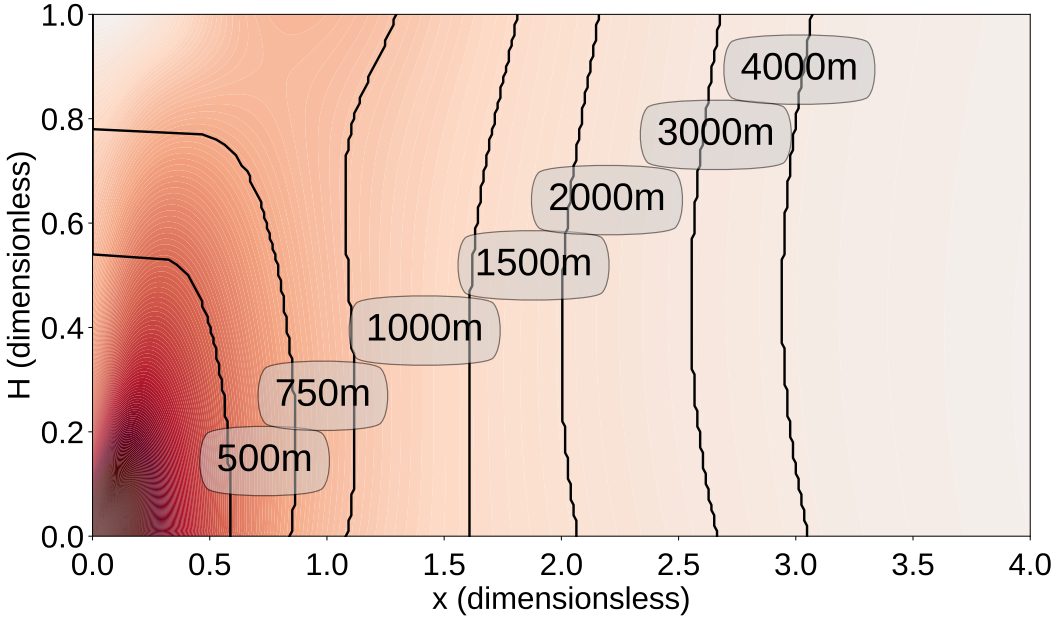

Figure 4. Outline of the failure region for different ice thicknesses on a dimensionless domain and without water stabilizing the front (ice thickness = glacier freeboard). The failure region is defined as region close to the calving front where the maximum shear stress exceeds the critical shear stress τ_c anywhere in the ice column.

Above a critical freeboard of about $1000\,\mathrm{m}$ the failure region encompasses the whole ice thickness. Below this critical value the failure region contains only the lower part of the ice thickness: but once the lower part of the ice column fails the upper part lacks support and fails as well. The freeobard - failure region relation has a bend at the critical freeboard and hence the two parts require separate analytical fits. Here, we consider only values below the critical freeboard because that is the range of values most likely to occur in nature.

In figure 5 we provide an analytical fit with a power law function of the form

$$L = \left(\frac{F - F_c}{F_s}\right)^s \mathrm{m} \tag{14}$$

$$F_s = \left(115 \cdot (w - 35.6\%)^4 + 21\right) \mathrm{m} \tag{15}$$

$$F_c = (75 - w \cdot 49)\ \mathrm{m} \tag{16}$$

$$s = 0.17 \cdot 9.1^w + 1.76 \tag{17}$$

with $w \equiv D/H < 0.9$ and $F \equiv H - D = H \cdot (1 - w)$

Fig. 5 shows the numerical results and the fit. Note that the fit has been optimized for relative error so for large freeboards the fit is a little off but it was considered more important to fit the onset of cliff calving correctly.

The Cryosphere Discuss., https://doi.org/10.5194/tc-2018-205
Manuscript under review for journal The Cryosphere
Discussion started: 11 October 2018

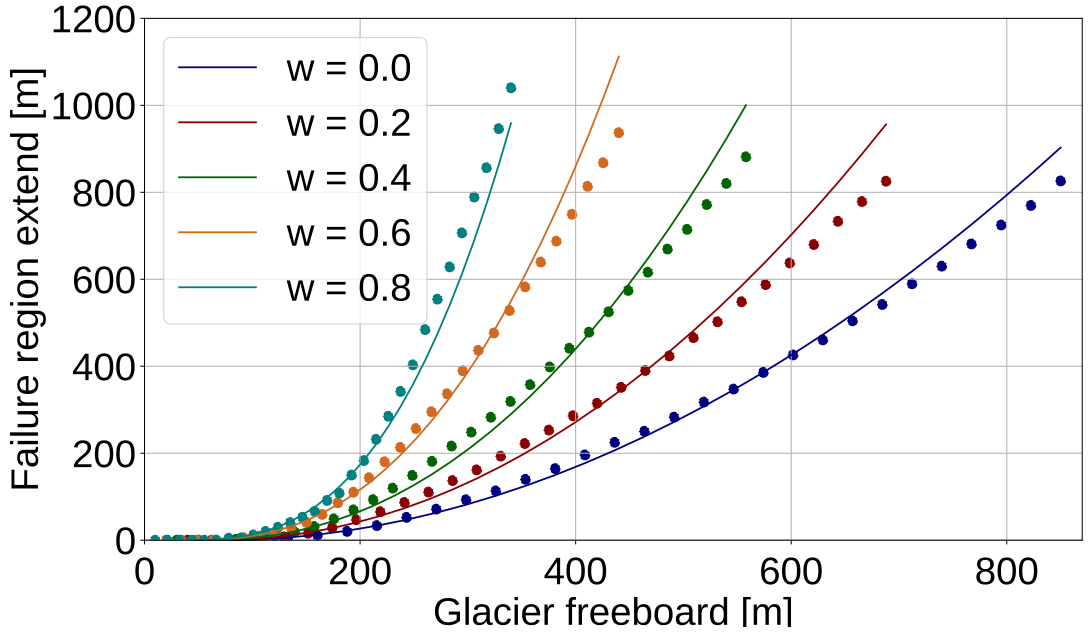

Figure 5. Size of shear failure region L as a function of glacier freeboard $F = H - D$ and relative water depth $w = D/H$, numerical results (round dots) and power law fit function (continuous line) eq. 14. The fit has been optimized for relative error in order to get the onset of cliff calving right.

5 Failure time

There is a theory for damage evolution in ice for tensile damage (Pralong et al., 2003), from which a time to failure can be derived (Mercenier et al., 2018):

$$T_f = \frac{(1-D_0)^{k+r+1} - (1-D_c)^{k+r+1}}{(k+r+1)B(\sigma_0 - \sigma_{th})^r} \tag{18}$$

with initial damage D_0, critical damage D_c and stress threshold for damage creation σ_{th} and the working stress σ_0 which we assume to be the maximum shear stress τ_{max}. However, this is strictly valid only for damages created through tensile creep. The difference between tensile and compressive damage is that in tension a single crack grows unstably to cause failure while in compression a large number of small crack grows stably until their interaction causes failure (Ashby and Sammis, 1990). There is plenty of literature about compressive creep and failure in rocks (Brantut et al., 2013). Fatigue failure happens when a material is loaded with stresses below the failure stress and fails with a time delay due to the development of micro cracks.

The Cryosphere Discuss., https://doi.org/10.5194/tc-2018-205
Manuscript under review for journal The Cryosphere
Discussion started: 11 October 2018

There is an exponential law and a power law for the time to failure:

$$t_f = t_0 \exp\left(-b\frac{\sigma}{\sigma_0}\right) \tag{19}$$

$$t_f = t_0' \left(\frac{\sigma}{\sigma_0}\right)^{b'} \tag{20}$$

The power law exponent is usually large, $b' \approx 20$, so the power law is very similar to the exponential law. Both fit the experimental data for rock well (Amitrano and Helmstetter, 2006). The constants depend on material properties. There are no studies for time dependence of compressive creep failure in ice.

Due to lack of data for time to failure in compressive failure of ice, we start with a time to failure as given by eq. 18,

$$T_f = \cdot(\sigma_0 - \sigma_{th})^{-r}/B \tag{21}$$

with $\sigma_{thr} = 0.17\,\mathrm{MPa}$, $r = 0.43$ and $B = 65\mathrm{Mpa}^{-r}\mathrm{a}^{-1}$, as given in Mercenier et al. (2018). These parameters have been determined by calibrating a tensile failure calving model with data on calving rate, water depth and ice thickness for a variety of tidewater glaciers in the Arctic.

For the stresses above the shear failure threshold, $\sigma_0 > 1\,\mathrm{MPa}$, the time to failure given by this relation changes by only a factor of 2 (see fig. 6). The calving relation can be further simplified by assuming, that there is a characteristic time to failure, T_c, that is the same for all stresses and sizes of failure regions, $T_c \approx 4\,\mathrm{days}$.

6 Calving law

With a constant failure time, the calving rate is proportional to the size of the failure region

$$C = C_0 \cdot \left(\frac{F - F_c}{F_s}\right)^s \tag{22}$$

$$F_s = \left(115 \cdot (w - 35.6\%)^4 + 21\right)\,\mathrm{m} \tag{23}$$

$$F_c = (75 - w \cdot 49)\,\mathrm{m} \tag{24}$$

$$s = 0.17 \cdot 9.1^w + 1.76 \tag{25}$$

$$C_0 = \frac{1\,\mathrm{m}}{4\,\mathrm{days}} = 91.25\,\mathrm{ma}^{-1} \tag{26}$$

with $w \equiv D/H < 0.9$ and $F \equiv H - D = H \cdot (1 - w)$.

How do cliff calving rates given by eq. 22 compare to currently observed calving rates? Jakobshavn glacier in Greenland is one of the few glacier that are currently in a cliff calving mode. It is difficult to determine calving rates directly, but if the grounding line were fixed, the calving rate would be equal to the ice flow velocity which is up to $12\,\mathrm{kma}^{-1}$ (Morlighem et al., 2014). The grounding line of Jakobshaven glacier retreats and advances seasonally about 6 km per year, but the maximum grounding line position has not changed much between 2012 and 2015 (Xie et al., 2018). So the averaged yearly calving rate

The Cryosphere Discuss., https://doi.org/10.5194/tc-2018-205
Manuscript under review for journal The Cryosphere
Discussion started: 11 October 2018

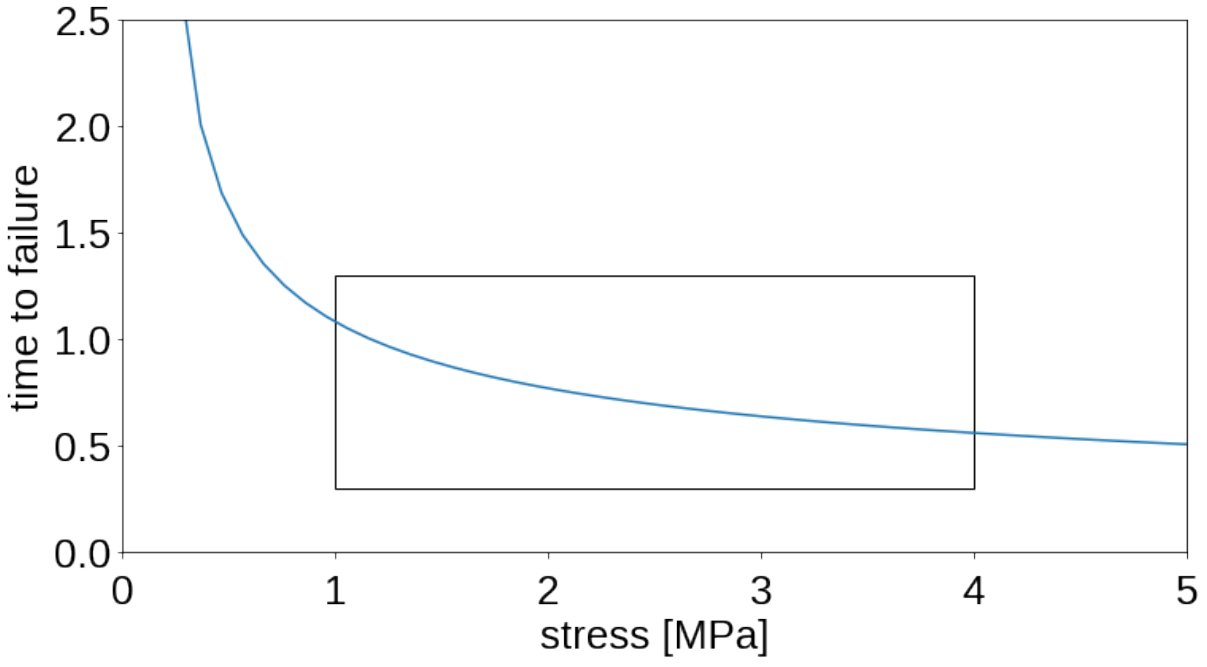

Figure 6. Time to failure given by eq. 21. For stresses above the shear failure threshold, $\sigma_0 > 1\,\mathrm{MPa}$, the time to failure changes only little (box).

w	s	F_c	F_s
0	1.93	75	22.85
0.1	1.97	70.1	21.49
0.2	2.02	65.2	21.07
0.3	2.09	60.3	21.00
0.4	2.17	55.4	21.00
0.5	2.27	50.5	21.05
0.6	2.40	45.6	21.41
0.7	2.56	40.7	22.61
0.8	2.75	35.8	25.47
0.9	3.00	30.9	31.07

Table 1. Table of parameters in the cliff calving relation eq. 22, giving the exponent s, critical freeboard F_c and scaling factor F_s for a range of relative water depth values w.

is approximately $12\,\mathrm{km a^{-1}}$.

Jakobshavn glacier terminates in water with a depth of 800 m (Morlighem et al., 2014) and has a glacier freeboard of 100 m (Xie et al., 2018). That brings Jakobshavn glacier in the cliff calving regime. Inserting these values into eq. 22 gives a cliff

The Cryosphere Discuss., https://doi.org/10.5194/tc-2018-205
Manuscript under review for journal The Cryosphere
Discussion started: 11 October 2018

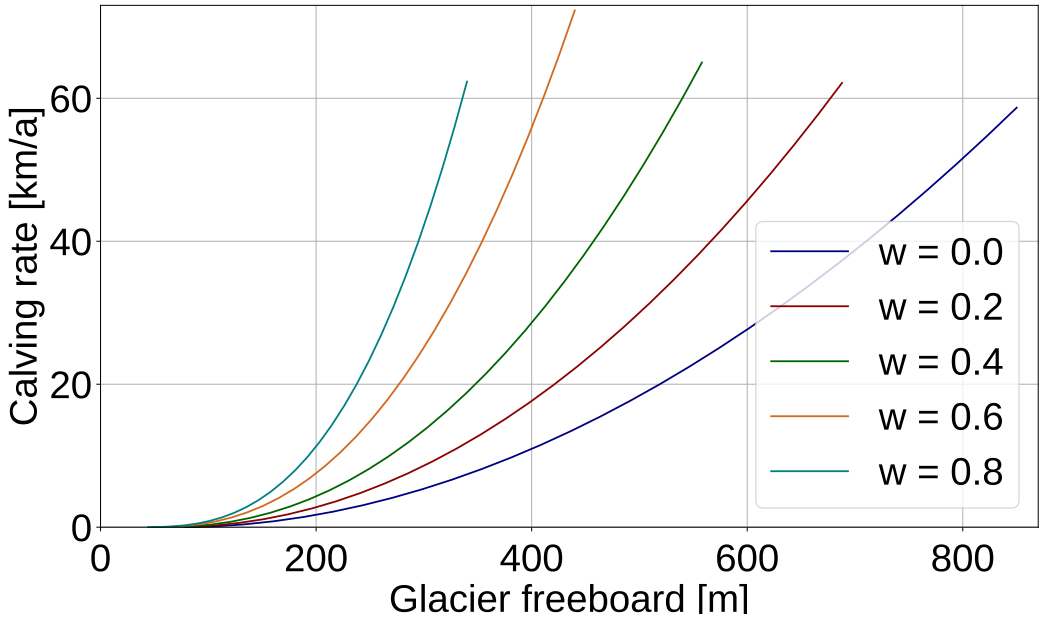

Figure 7. Cliff calving rates C as a function of glacier freeboard $F = H - D$ and relative water depth $w = D/H$ as given by eq. 22.

calving rate of $C = 750\,\mathrm{m a}^{-1}$, which is well below the overall calving rate. Jakoshavn glacier is heavily crevassed so other calving mechanism are likely to play a role and the cliff calving rate is only a part of the whole calving rate.

6.1 Discussion and Conclusion

We solved the 2D Stokes equation numerically for a flat glacier frozen to its bed in a flowline model and investigated the stresses at the calving front.

Four simplifications were made:

1. The model was solved in one horizontal direction, neglecting lateral shear effects. Without lateral shear effects, the result is indepenent of the topography of individual glaciers.
2. We assumed a basal boundary condition corresponding to a glacier frozen to its bed. Sliding was not considered.
3. The main failure mechanism was assumed to be shear faulting without friction compared to the Coulomb law, where friction which ice cliffs. Friction would allow glaciers with larger freeboards than observed to be stable.
4. A constant time to failure has been assumed.

Under these assumptions, crevasses cannot penetrate the whole glacier depth and shear failure was chosen as the main failure mechanism. The region where shear stresses exceed a critical shear stress of 1 MPa is called the failure region. The extend of this failure region was determined for a range of glacier freeboards and relative water depths. Where the failure region does not encompass the whole ice thickness, an analytical fit was made. Assuming a constant time to failure, a cliff calving rate was derived. Resulting cliff calving rates seem large compared to currently observed calving rates, but comparison with Jakobshavn glacier in Greenland, where cliff calving contributes to the overall calving rate, shows that it can be realistic. However, cliff calving rates increase quickly with increasing glacier freeboard and glaciers in a true cliff calving regime can retreat much faster than has been observed so far.

The calving law proposed here was derived under a number of constraining assumptions. First it was assumed that friction plays no role in shear failure. Secondly it was assumed that once the critical shear stress is exceeded, ice fails after a constant time to failure. An improved cliff calving model might include friction and allow a stress-dependent time to failure.
If the Coulomb law with a friction component is used, the immediate failure region is smaller than in the no-friction case. Time to failure relations for compressive failure as given by 19 and 20 are valid for stresses below the critical shear stress. Failure is assumed to be instantaneous as soon as the critical shear stress is reached. Regions where the stress is below the failure stress would be assigned a stress-dependent failure time leading to a spatially distributed time to failure. Since friction is smaller at the top of the ice cliff, the top would fail earlier than the base, leaving a foot that would subsequently fail due to buoyant forces. There is no simple way to find a parametrization of the cliff calving rate for these processes. Another problem is that there are no laboratory studies on the paramaters in the time to failure relations for ice. It is also not possible to calibrate the calving relation using observed calving rates, because there are no glaciers currently available where cliff calving is the primary failure mechanism. Paleorecords might provide some means to calibrate cliff-calving rates as attempted in Pollard et al. (2015) and DeConto and Pollard (2016).

Paleorecords might not be constraining enough to provide a useful limit for the Antarctic sea level contribution of the next 85 years. But even if it is difficult to constrain the rate of cliff-calving there are important qualitative consequences of a monotonously increasing cliff-calving dependence on ice thickness. The most important is the potential of a self-amplifying ice loss mechanism which is not constraint by the reduction in calving but must be constraint by other processes. Without some kind of cliff-calving mechanism it is likely that ice sheet models are lacking an important ice loss mechanism.

Code availability. FeniCS can be downloaded from the project website https://fenicsproject.org/download/. The script used for the FeniCS simulation in this paper is available on request from the authors.

The Cryosphere Discuss., https://doi.org/10.5194/tc-2018-205
Manuscript under review for journal The Cryosphere
Discussion started: 11 October 2018

Appendix A: Simplified stress balance

It is possible to solve the stress balance at the calving front analytically in a depth-averaged model with a simplifying assumption for the isotropic pressure. This has been used by (Bassis and Walker, 2011) and (Pollard et al., 2015). It is interesting to compare this with the numerical stress field solution obtained above.

(Bassis and Walker, 2011) and (Pollard et al., 2015) assumed the isotropic pressure is given by the gravitational pressure

$$P(x,z) = \rho_i g(H - z) \tag{A1}$$

where ρ_i is the density of ice. This assumption is actually only true over length scales that are large compared with the ice thickness and far from the ice margins (MacAyeal, 1989), which is not the case when stresses close to the calving front are analysed. But making this assumption allows for an analytical solution of the depth-averaged stresses and does not require any ice rheology.

Together with incrompessibilty, which means that the trace of the strain rate disappears ($\dot{\epsilon}_{kk} = 0$) and implies $S_{xx} + S_{zz} = 0$, the 2D Stokes equations become:

$$0 = \frac{\partial S_{xx}}{\partial x} + \frac{\partial S_{xz}}{\partial z}\,, \tag{A2}$$

$$0 = \frac{\partial S_{xz}}{\partial x} - \frac{\partial S_{xx}}{\partial z}\,. \tag{A3}$$

Assuming a tractionfree surface boundary, traction-continuity at the terminus boundary and vanishing deviatoric stresses at the upstream boundary as well as the bed boundary, a boundary value problem arises that can be solved numerically.

The resulting stresses are smaller than the stresses obtained in the section 2 for the 2D Stokes equation with nonlinear ice rheology (figure A1). A failure region can be defined as in section 3 and its size shows a very similar dependence on glacier freeboard and water depth, though it is smaller by about a factor of three.

The biggest difference between the two approaches lies in the largest principal stress: In this simplified problem, the largest principal stress is negative in the whole ice volume; there is no region of tensile stresses, so no crevasses form. This is due to the assumption that the isotropic pressure is equal to the gravitational pressure, which is not actually the case in the vicinity of the glacier terminus.

A1

Competing interests. The authors declare no competing interests.

The Cryosphere Discuss., https://doi.org/10.5194/tc-2018-205
Manuscript under review for journal The Cryosphere
Discussion started: 11 October 2018

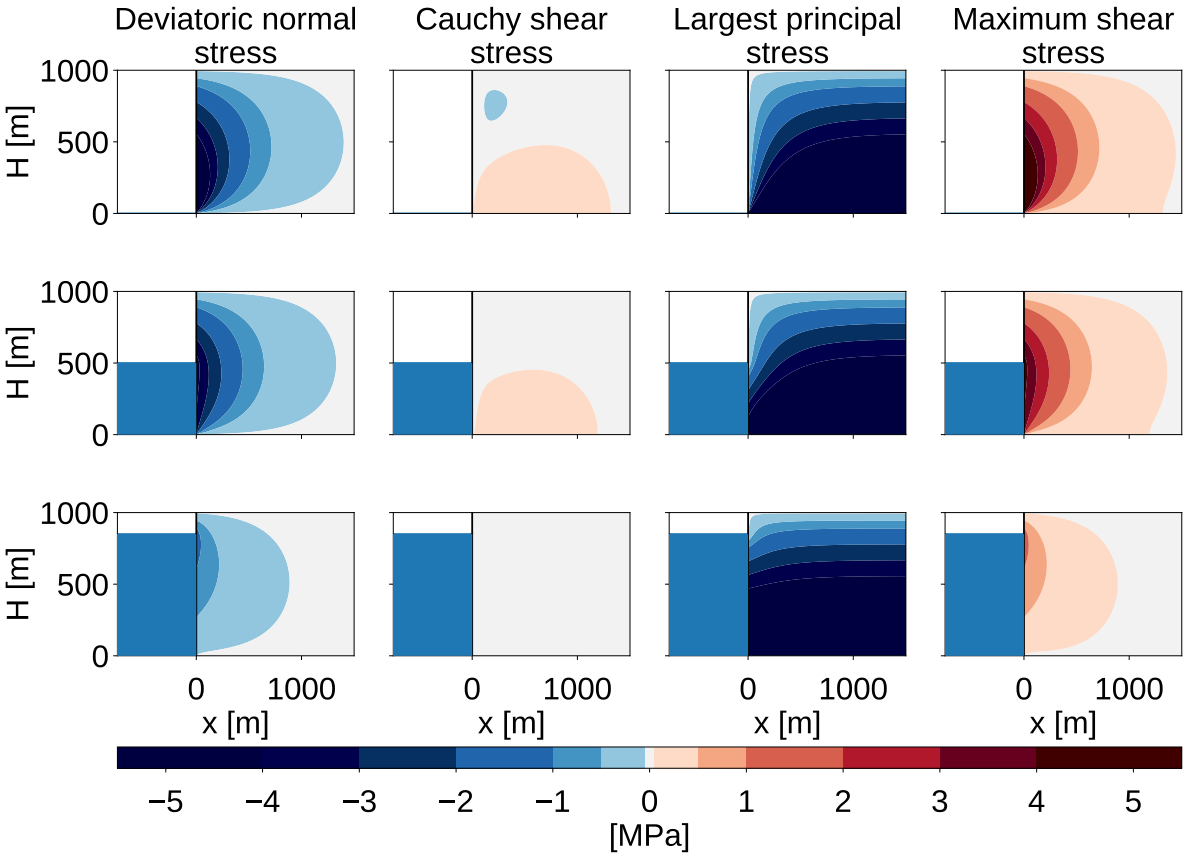

Figure A1. Stress configurations at the calving front for different relative water depths ($w = 0, 0.5, 0.85$) for a fixed ice thickness of 1000m. The first row shows the deviatoric normal stress in x-direction, S_{xx}, the second row shows the Cauchy shear stress, $\sigma_{xz} = S_{xz}$, the third row shows the largest principal stress, σ_i, and the last row shows the maximum shear stress, τ_{max}.

Acknowledgements. TS was funded by the Heinrich Böll Foundation. TS would like to thank Yue Ma and Christian Helanow for their valuable help with FeniCS.

References

Alnæs, M. S., Blechta, J., Hake, J., Johansson, A., Kehlet, B., Logg, A., Richardson, C., Ring, J., Rognes, M. E., and Wells, G. N.: The FEniCS Project Version 1.5, Archive of Numerical Software, 3, https://doi.org/10.11588/ans.2015.100.20553, 2015.

Amitrano, D. and Helmstetter, A.: Brittle creep, damage, and time to failure in rocks, Journal of Geophysical Research: Solid Earth, 111, https://doi.org/10.1029/2005JB004252, https://agupubs.onlinelibrary.wiley.com/doi/abs/10.1029/2005JB004252, 2006.

Ashby, M. F. and Sammis, C. G.: The damage mechanics of brittle solids in compression, pure and applied geophysics, 133, 489–521, https://doi.org/10.1007/BF00878002, https://doi.org/10.1007/BF00878002, 1990.

Bassis, J. N. and Walker, C. C.: Upper and lower limits on the stability of calving glaciers from the yield strength envelope of ice, Proceedings of the Royal Society of London A: Mathematical, Physical and Engineering Sciences, https://doi.org/10.1098/rspa.2011.0422, http://rspa.royalsocietypublishing.org/content/early/2011/11/17/rspa.2011.0422, 2011.

Benn, D., Astrom, J., Zwinger, T., Todd, J., Nick, F., Cook, S., Hulton, N., and Luckmann, A.: Melt-under-cutting and buoyancy-driven calving from tidewater glaciers: new insights from discrete element and continuum model simulations, Journal of Glaciology, 63, 691–702, https://doi.org/10.1017/jog.2017.41, 2017.

Benn, D. I., Warren, C. R., and Mottram, R. H.: Calving processes and the dynamics of calving glaciers, Earth-Science Reviews, 82, 143–179, https://doi.org/10.1016/j.earscirev.2007.02.002, http://www.sciencedirect.com/science/article/pii/S0012825207000396, 2007.

Brantut, N., Heap, M., Meredith, P., and Baud, P.: Time-dependent cracking and brittle creep in crustal rocks: A review, Journal of Structural Geology, 52, 17 – 43, https://doi.org/https://doi.org/10.1016/j.jsg.2013.03.007, http://www.sciencedirect.com/science/article/pii/S0191814113000473, 2013.

Church, J. A., Clark, P. U., Cazenave, A., Gregory, J. M., Jevrejeva, S., Levermann, A., Merrifield, M. A., Milne, G. A., Nerem, R. S., Nunn, P. D., Payne, A. J., Pfeffer, W. T., Stammer, D., and Unnikrishnan, A. S.: Sea-Level Rise by 2100, Science, 342, 1445–1445, https://doi.org/10.1126/science.342.6165.1445-a, http://science.sciencemag.org/content/342/6165/1445.1, 2013.

Das, S. B., Joughin, I., Behn, M. D., Howat, I. M., King, M. A., Lizarralde, D., and Bhatia, M. P.: Fracture Propagation to the Base of the Greenland Ice Sheet During Supraglacial Lake Drainage, Science, 320, 778–781, https://doi.org/10.1126/science.1153360, http://science.sciencemag.org/content/320/5877/778, 2008.

DeConto, R. M. and Pollard, D.: Contribution of Antarctica to past and future sea-level rise, Nature, 531, 591–597, https://doi.org/http://dx.doi.org/10.1038/nature17145 10.1038/nature17145, http://www.nature.com/nature/journal/v531/n7596/abs/nature17145.html#supplementary-information, 2016.

Depoorter, M. A., Bamber, J. L., Griggs, J. A., Lenaerts, J. T. M., Ligtenberg, S. R. M., van den Broeke, M. R., and Moholdt, G.: Calving fluxes and basal melt rates of Antarctic ice shelves, Nature, 502, 89, http://dx.doi.org/10.1038/nature12567, 2013.

Enderlin, E. M., Howat, I. M., Jeong, S., Noh, M.-J., Angelen, J. H., and Broeke, M. R.: An improved mass budget for the Greenland ice sheet, Geophysical Research Letters, 41, 866–872, https://doi.org/10.1002/2013GL059010, https://agupubs.onlinelibrary.wiley.com/doi/abs/10.1002/2013GL059010, 2014.

Ford, H. and Alexander, J. M.: Advanced mechanics of materials, 1963.

Joughin, I. and MacAyeal, D. R.: Calving of large tabular icebergs from ice shelf rift systems, Geophysical Research Letters, 32, n/a–n/a, https://doi.org/10.1029/2004GL020978, http://dx.doi.org/10.1029/2004GL020978, l02501, 2005.

Kopp, R. E., DeConto, R. M., Bader, D. A., Hay, C. C., Horton, R. M., Kulp, S., Oppenheimer, M., Pollard, D., and Strauss, B. H.: Evolving Understanding of Antarctic Ice-Sheet Physics and Ambiguity in Probabilistic Sea-Level Projections, Earth's Future, 5, 1217–1233, https://doi.org/10.1002/2017EF000663, https://agupubs.onlinelibrary.wiley.com/doi/abs/10.1002/2017EF000663.

Lazzara, M. A., Jezek, K. C., Scambos, T. A., MacAyeal, D. R., and van der Veen, C. J.: On the recent calving of icebergs from the Ross Ice Shelf, Polar Geography, 23, 201–212, https://doi.org/10.1080/10889379909377676, http://dx.doi.org/10.1080/10889379909377676, 1999.

Levermann, A., Winkelmann, R., Nowicki, S., Fastook, J. L., Frieler, K., Greve, R., Hellmer, H. H., Martin, M. A., Meinshausen, M., Mengel, M., Payne, A. J., Pollard, D., Sato, T., Timmermann, R., Wang, W. L., and Bindschadler, R. A.: Projecting Antarctic ice discharge using response functions from SeaRISE ice-sheet models, Earth System Dynamics, 5, 271–293, https://doi.org/10.5194/esd-5-271-2014, https://www.earth-syst-dynam.net/5/271/2014/, 2014.

Ma, Y., Tripathy, C. S., and Bassis, J. N.: Bounds on the calving cliff height of marine terminating glaciers, Geophysical Research Letters, 44, 1369–1375, https://doi.org/10.1002/2016GL071560, http://dx.doi.org/10.1002/2016GL071560, 2016GL071560, 2017.

MacAyeal, D. R.: Large-scale ice flow over a viscous basal sediment: Theory and application to ice stream B, Antarctica, Journal of Geophysical Research: Solid Earth, 94, 4071–4087, https://doi.org/10.1029/JB094iB04p04071, http://dx.doi.org/10.1029/JB094iB04p04071, 1989.

Meier, M. F. and Post, A.: Fast tidewater glaciers, Journal of Geophysical Research: Solid Earth, 92, 9051–9058, https://doi.org/10.1029/JB092iB09p09051, http://dx.doi.org/10.1029/JB092iB09p09051, 1987.

Mengel, M., Feldmann, J., and Levermann, A.: Linear sea-level response to abrupt ocean warming of major West Antarctic ice basin, Nature Climate Change, 6, 71, http://dx.doi.org/10.1038/nclimate2808, 2016.

Mercenier, R., Lüthi, M. P., and Vieli, A.: Calving relation for tidewater glaciers based on detailed stress field analysis, The Cryosphere, 12, 721–739, https://doi.org/10.5194/tc-12-721-2018, https://www.the-cryosphere.net/12/721/2018/, 2018.

Morlighem, M., Rignot, E., Mouginot, J., Seroussi, H., and Larour, E.: Deeply incised submarine glacial valleys beneath the Greenland ice sheet, Nature Geoscience, 7, 418, http://dx.doi.org/10.1038/ngeo2167, 2014.

Morlighem, M., Bondzio, J., Seroussi, H., Rignot, E., Larour, E., Humbert, A., and Rebuffi, S.: Modeling of Store Gletscher's calving dynamics, West Greenland, in response to ocean thermal forcing, Geophysical Research Letters, 43, 2659–2666, https://doi.org/10.1002/2016GL067695, http://dx.doi.org/10.1002/2016GL067695, 2016GL067695, 2016.

Nick, F., van der Veen, C., Vieli, A., and Benn, D.: A physically based calving model applied to marine outlet glaciers and implications for the glacier dynamics, Journal of Glaciology, 56, 781–794, https://doi.org/doi:10.3189/002214310794457344, http://www.ingentaconnect.com/content/igsoc/jog/2010/00000056/00000199/art00004, 2010.

Nye, J. F.: The Distribution of Stress and Velocity in Glaciers and Ice-Sheets, Proceedings of the Royal Society of London A: Mathematical, Physical and Engineering Sciences, 239, 113–133, https://doi.org/10.1098/rspa.1957.0026, http://rspa.royalsocietypublishing.org/content/239/1216/113, 1957.

Pollard, D., DeConto, R. M., and Alley, R. B.: Potential Antarctic Ice Sheet retreat driven by hydrofracturing and ice cliff failure, Earth and Planetary Science Letters, 412, 112 – 121, https://doi.org/http://dx.doi.org/10.1016/j.epsl.2014.12.035, http://www.sciencedirect.com/science/article/pii/S0012821X14007961, 2015.

Pralong, A. and Funk, M.: Dynamic damage model of crevasse opening and application to glacier calving, Journal of Geophysical Research (Solid Earth), 110, B01 309, https://doi.org/10.1029/2004JB003104, 2005.

Pralong, A., Funk, M., and Lüthi, M. P.: A description of crevasse formation using continuum damage mechanics, Annals of Glaciology, 37, 77–82, 2003.

Rignot, E. and Kanagaratnam, P.: Changes in the Velocity Structure of the Greenland Ice Sheet, Science, 311, 986–990, https://doi.org/10.1126/science.1121381, http://science.sciencemag.org/content/311/5763/986, 2006.

Rignot, E., Mouginot, J., Morlighem, M., Seroussi, H., and Scheuchl, B.: Widespread, rapid grounding line retreat of Pine Island, Thwaites, Smith, and Kohler glaciers, West Antarctica, from 1992 to 2011, Geophysical Research Letters, 41, 3502–3509, https://doi.org/10.1002/2014GL060140, http://dx.doi.org/10.1002/2014GL060140, 2014.

Ritz, C., Edwards, Tamsin L., Durand, Gaël, Payne, Antony J., Peyaud, Vincent, and Hindmarsh, Richard C. A.: Potential sea-level rise from Antarctic ice-sheet instability constrained by observations, Nature, 528, 115–118, https://doi.org/http://dx.doi.org/10.1038/nature16147 10.1038/nature16147, http://www.nature.com/nature/journal/v528/n7580/abs/nature16147.html#supplementary-information, 2015.

Schulson, E. M.: Brittle failure of ice, Engineering Fracture Mechanics, 68, 1839 – 1887, https://doi.org/http://dx.doi.org/10.1016/S0013-7944(01)00037-6, http://www.sciencedirect.com/science/article/pii/S0013794401000376, 2001.

Schulson, E. M., Iliescu, D., and Renshaw, C. E.: On the initiation of shear faults during brittle compressive failure: A new mechanism, Journal of Geophysical Research: Solid Earth, 104, 695–705, https://doi.org/10.1029/1998JB900017, http://dx.doi.org/10.1029/1998JB900017, 1999.

Shepherd, A., Ivins, E., Rignot, E., Smith, B., van den Broeke, M., Velicogna, I., Whitehouse, P., Briggs, K., Joughin, I., Krinner, G., Nowicki, S., Payne, T., Scambos, T., Schlegel, N., Geruo, A., Agosta, C., Ahlstrøm, A., Babonis, G., Barletta, V., Blazquez, A., Bonin, J., Csatho, B., Cullather, R., Felikson, D., Fettweis, X., Forsberg, R., Gallee, H., Gardner, A., Gilbert, L., Groh, A., Gunter, B., Hanna, E., Harig, C., Helm, V., Horvath, A., Horwath, M., Khan, S., Kjeldsen, K. K., Konrad, H., Langen, P., Lecavalier, B., Loomis, B., Luthcke, S., McMillan, M., Melini, D., Mernild, S., Mohajerani, Y., Moore, P., Mouginot, J., Moyano, G., Muir, A., Nagler, T., Nield, G., Nilsson, J., Noel, B., Otosaka, I., Pattle, M. E., Peltier, W. R., Pie, N., Rietbroek, R., Rott, H., Sandberg-Sørensen, L., Sasgen, I., Save, H., Scheuchl, B., Schrama, E., Schröder, L., Seo, K.-W., Simonsen, S., Slater, T., Spada, G., Sutterley, T., Talpe, M., Tarasov, L., van de Berg, W. J., van der Wal, W., van Wessem, M., Vishwakarma, B. D., Wiese, D., Wouters, B., and team, T. I. M. B. I. E.: Mass balance of the Antarctic Ice Sheet from 1992 to 2017, Nature, 558, 219–222, https://doi.org/10.1038/s41586-018-0179-y, 2018.

Slangen, A. B. A., Adloff, F., Jevrejeva, S., Leclercq, P. W., Marzeion, B., Wada, Y., and Winkelmann, R.: A Review of Recent Updates of Sea-Level Projections at Global and Regional Scales, pp. 395–416, Springer International Publishing, Cham, https://doi.org/10.1007/978-3-319-56490-6_17, https://doi.org/10.1007/978-3-319-56490-6_17, 2017.

Todd, J., Christoffersen, P., Zwinger, T., Råback, P., Chauché, N., Benn, D., Luckman, A., Ryan, J., Toberg, N., Slater, D., and Hubbard, A.: A Full-Stokes 3-D Calving Model Applied to a Large Greenlandic Glacier, Journal of Geophysical Research: Earth Surface, 123, 410–432, https://doi.org/10.1002/2017JF004349, https://agupubs.onlinelibrary.wiley.com/doi/abs/10.1002/2017JF004349, 2018.

van der Veen, C. J.: Fundamentals of Glacier Dynamics, A.A. Balkema, 1999.

van Der Veen, J.: Tidewater calving, Journal of Glaciology, 42, 375–385, https://doi.org/doi:10.3198/1996JoG42-141-375-385, http://www.ingentaconnect.com/content/igsoc/jog/1996/00000042/00000141/art00018, 1996.

Vieli, A., Jania, J., and Kolondra, L.: The retreat of a tidewater glacier: observations and model calculations on Hansbreen, Spitsbergen, Journal of Glaciology, 48, 592–600, https://doi.org/doi:10.3189/172756502781831089, http://www.ingentaconnect.com/content/igsoc/jog/2002/00000048/00000163/art00013, 2002.

Walter, F., O'Neel, S., McNamara, D., Pfeffer, W. T., Bassis, J. N., and Fricker, H. A.: Iceberg calving during transition from grounded to floating ice: Columbia Glacier, Alaska, Geophysical Research Letters, 37, n/a–n/a, https://doi.org/10.1029/2010GL043201, http://dx.doi.org/10.1029/2010GL043201, 2010.

WCRP Global Sea Level Budget Group: Global sea-level budget 1993–present, Earth System Science Data, 10, 1551–1590, https://doi.org/10.5194/essd-10-1551-2018, https://www.earth-syst-sci-data.net/10/1551/2018/, 2018.

Weertman, J.: Can a water-filled crevasse reach the bottom surface of a glacier, IASH Publ, 95, 139–145, 1973.

Weiss, J. and Schulson, E. M.: Coulombic faulting from the grain scale to the geophysical scale: lessons from ice, Journal of Physics D: Applied Physics, 42, 214 017, http://stacks.iop.org/0022-3727/42/i=21/a=214017, 2009.

Xie, S., Dixon, T. H., Voytenko, D., Deng, F., and Holland, D. M.: Grounding line migration through the calving season at Jakobshavn Isbræ, Greenland, observed with terrestrial radar interferometry, The Cryosphere, 12, 1387–1400, https://doi.org/10.5194/tc-12-1387-2018, https://www.the-cryosphere.net/12/1387/2018/, 2018.

Zhang, H., Ju, L., Gunzburger, M., Ringler, T., and Price, S.: Coupled Models and Parallel Simulations for Three-Dimensional Full-Stokes Ice Sheet Modeling, Numerical Mathematics: Theory, Methods and Applications, 4, 396–418, https://doi.org/10.1017/S1004897900000416, 2011.